JACS
JOURNAL OF THE AMERICAN CHEMICAL SOCIETY
Article
pubs.acs.org/JACS

Ruthenium-Catalyzed Asymmetric Hydrohydroxyalkylation of Butadiene: The Role of the Formyl Hydrogen Bond in Stereochemical Control

Matthew N. Grayson,[†] Michael J. Krische,[‡] and K. N. Houk*[,†]

[†]Department of Chemistry and Biochemistry, University of California, Los Angeles, California 90095-1569, United States
[‡]Department of Chemistry and Biochemistry, University of Texas at Austin, Austin, Texas 78712, United States

Supporting Information

ABSTRACT: The catalyst generated in situ from $RuH_2(CO)(PPh_3)_3$, (*S*)-SEGPHOS, and a chiral phosphoric acid promotes asymmetric hydrohydroxyalkylation of butadiene and affords enantioenriched α-methyl homoallylic alcohols. The observed diastereo- and enantioselectivities are determined by both the chiral phosphine and chiral phosphate ligands. Density functional theory calculations (M06/SDD-6-311G(d,p)−IEFPCM(acetone)//B3LYP/SDD-6-31G(d)) predict that the product distribution is controlled by the kinetics of carbon−carbon bond formation, and this process occurs via a closed-chair Zimmerman−Traxler-type transition structure (TS). Chiral-phosphate-dependent stereoselectivity arising from this TS is enabled through a hydrogen bond between the phosphoryl oxygen and the aldehyde formyl proton present in TADDOL-derived catalysts. This interaction is absent in the corresponding BINOL-derived systems, and the opposite diastereo- and enantioselectivity is observed. Additional factors influencing the stereochemical control are determined.

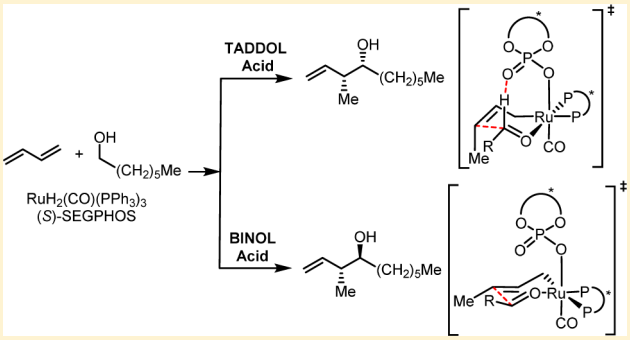

1. INTRODUCTION

The introduction of crotyl (α-methylallyl) groups into organic molecules is an important type of stereoselective carbon−carbon bond formation.[1,2] Crotylation of carbonyl compounds introduces multiple stereogenic centers, and the double bond of the resulting α-methyl homoallylic alcohol is a useful synthetic handle.[3] This type of reaction has been used extensively in polyketide natural product synthesis.[4,5] Many different asymmetric methods exist to synthesize α-methyl homoallylic alcohols, but these typically rely upon either substrate or reagent control.[6,7] Crotylboration of aldehydes is a typical example (Scheme 1).

Scheme 1. Example of Reagent-Controlled Crotylation of Carbonyl Compounds[8,9]

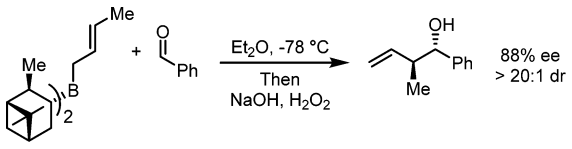

Krische's ruthenium-catalyzed asymmetric hydrohydroxyalkylation of butadiene is an alternate strategy for crotylation of carbonyl compounds. It has the advantage of bypassing the use of chiral premetalated reagents. The catalyst generated in situ from $RuH_2(CO)(PPh_3)_3$, dppf, and a BINOL-derived phosphoric acid promotes asymmetric hydrohydroxyalkylation of butadiene and affords enantioenriched α-methyl homoallylic alcohols with good levels of anti diastereoselectivity (Scheme 2).[10] Furthermore, by using the catalyst system derived from $RuH_2(CO)(PPh_3)_3$, (*S*)-SEGPHOS, and a chiral phosphoric acid, the diastereoselectivity can be controlled by changing the chiral phosphoric acid (Scheme 3).[11] Catalyst systems generated from TADDOL-derived phosphate ligand **1a** delivered α-methyl homoallylic alcohols with good levels of *syn*-diastereoselectivity and high levels of enantioselectivity. Match/mismatch effects between the chiral phosphate ligand **1b** and the chiral phosphine

Scheme 2. Ruthenium-Catalyzed Diastereo- and Enantioselective Hydrohydroxyalkylation of Butadiene[10]

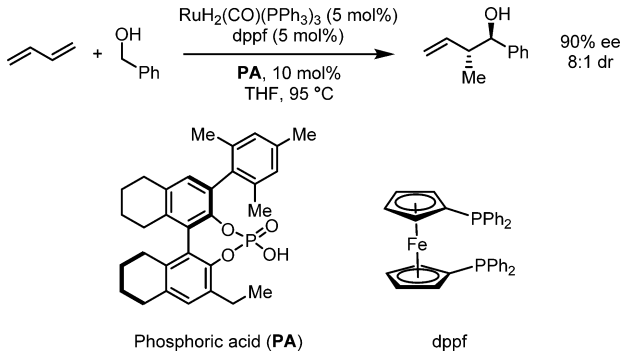

Received: May 9, 2015
Published: June 24, 2015

DOI: 10.1021/jacs.5b04844
J. Am. Chem. Soc. 2015, 137, 8838−8850

Scheme 3. Chiral-Phosphate-Dependent Stereoselectivity in the Ruthenium-Catalyzed Diastereo- and Enantioselective Hydrohydroxyalkylation of Butadiene[11]

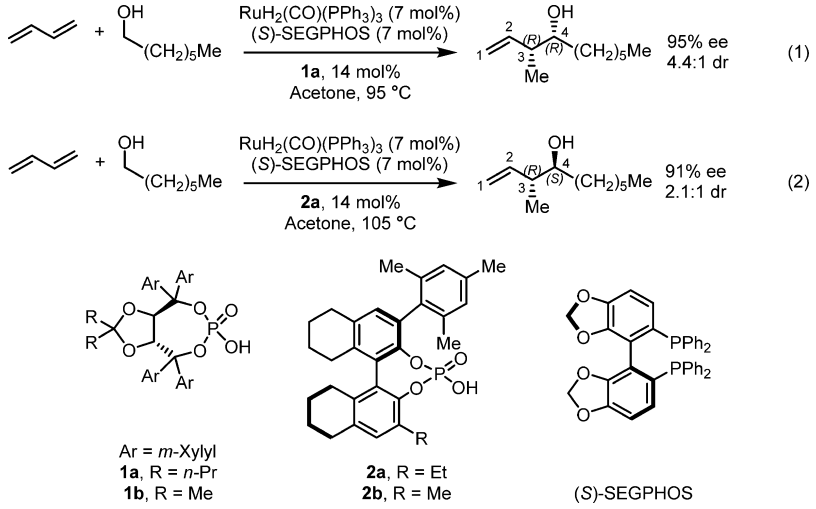

Scheme 4. Proposed Catalytic Cycle[10,11]

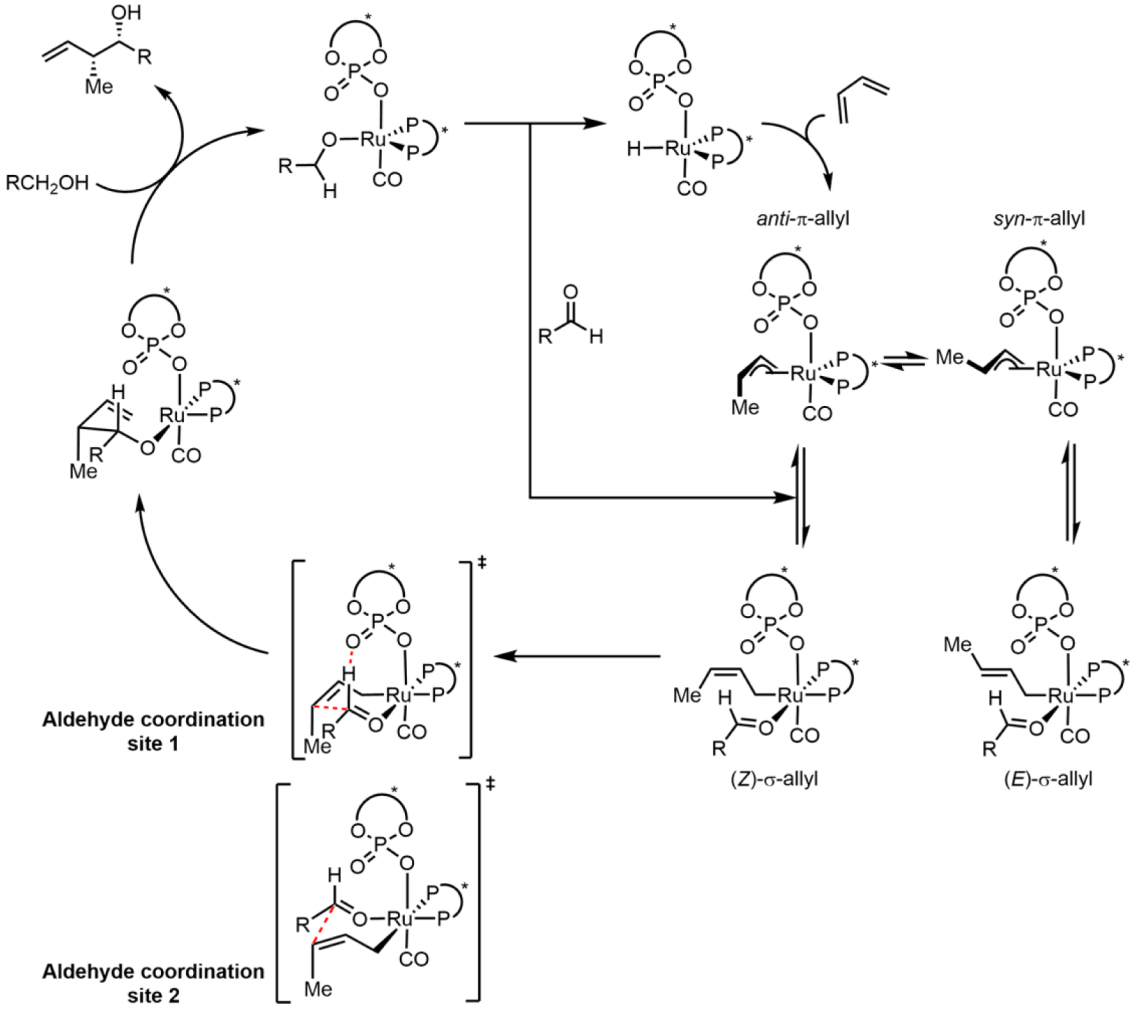

ligands (*R*)- and (*S*)-SEGPHOS also impact the enantioselectivity (*vide infra*). Catalyst systems generated from H_8-BINOL-derived phosphate **2a** led to *anti*-diastereoselectivity and attack on the opposite face of the prochiral aldehyde. The origins of this unexpected chiral-phosphate-dependent stereoselectivity were unknown but are the subject of the computational investigation reported here.

Scheme 4 shows the proposed catalytic cycle for ruthenium-catalyzed asymmetric hydrohydroxyalkylation of butadiene.[10,11] A computational study of an achiral iridium-catalyzed process by

DOI: 10.1021/jacs.5b04844
J. Am. Chem. Soc. 2015, 137, 8838−8850

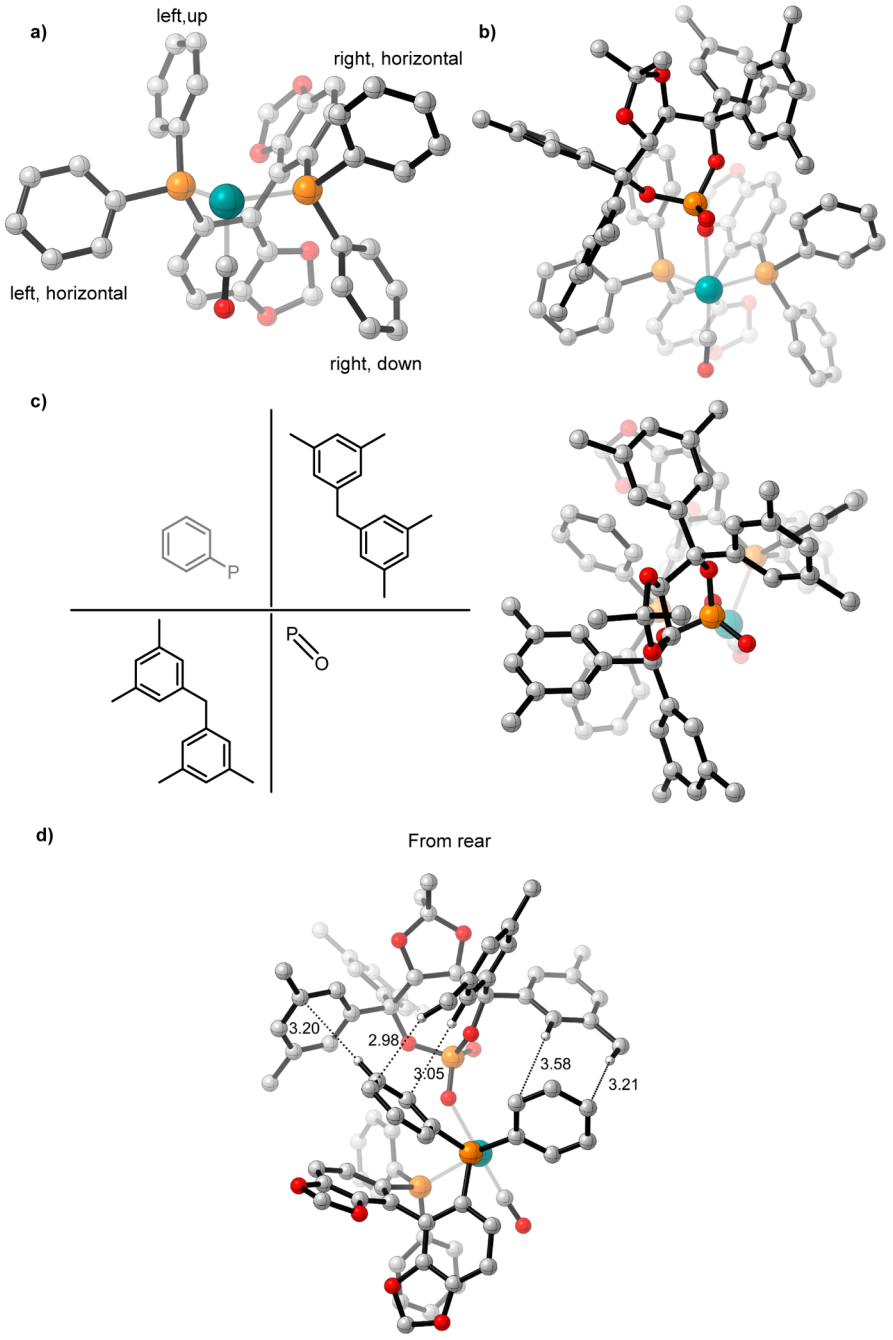

Figure 1. (a) (*S*)-SEGPHOS bound to ruthenium. (b) TADDOL-derived phosphate and its slanted orientation relative to the P−Ru−P plane. (c) Catalyst system viewed from above. The catalyst's conformational rigidity is in part due to a SEGPHOS phenyl group that occupies an empty quadrant of the TADDOL-derived scaffold (top left), preventing phosphate rotation. (d) Network of CH−π interactions. All of the structures are derived from optimized *syn*-π-allyl species; noncritical atoms have been omitted for clarity. M06/SDD-6-311G(d,p)−IEFPCM(acetone)//B3LYP/SDD-6-31G(d).

Li and Wang supports this cycle.[12] As shown in Scheme 4, *syn*-π- and *anti*-π-crotylruthenium isomers yield the (*E*)- and (*Z*)-σ-crotylruthenium species, respectively. The π-allyl species can isomerize through an $\eta^3-\eta^1-\eta^3$-type process ($\pi-\sigma-\pi$ allyl isomerization).[13,14] Given a rapidly interconverting mixture of π-allyl species, C−C bond formation via a closed-chair Zimmerman−Traxler-type transition structure (TS) is expected to yield *anti*-diastereoselectivity as a result of preferential reaction of the (*E*)-σ isomer, which places both the methyl group and the aldehyde substituent pseudoequatorial in the TS.[15] Therefore, the unexpected *syn*-diastereoselectivity observed with TADDOL-derived phosphates was suggested to arise from slow isomerization between π-crotylruthenium isomers. Such a mechanism would deliver exclusively the (*Z*)-σ-crotylruthenium isomer from the *anti*-π-crotylruthenium species after the kinetically preferred hydrometalation of the s-*cis* conformer of butadiene.[11]

However, experimental evidence suggests this isomerization is rapid under the reaction conditions and that the final product distribution is controlled by the kinetics of C−C bond formation.[16−18] After C−C bond formation, the resulting homoallylic ruthenium alkoxide exchanges with a reactant alcohol to release the product. The catalytic cycle is closed by dehydrogenation to form the aldehyde and regenerate the ruthenium hydride.[10]

DOI: 10.1021/jacs.5b04844
J. Am. Chem. Soc. 2015, 137, 8838−8850

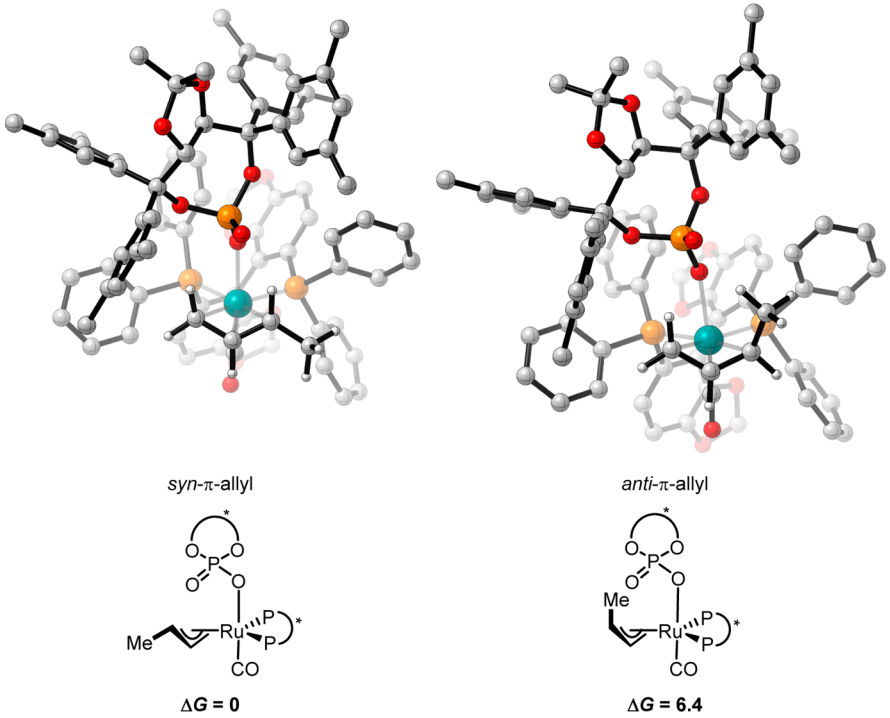

Figure 2. Lowest-energy *syn*- and *anti*-π-crotylruthenium isomers in reaction 1. M06/SDD-6-311G(d,p)−IEFPCM(acetone)//B3LYP/SDD-6-31G(d). Noncritical hydrogen atoms have been omitted for clarity. All free energies are in kcal mol^{-1}.

We have carried out density functional theory (DFT) calculations which show that the product distribution is controlled by the kinetics of carbon−carbon bond formation. This process occurs via a closed-chair Zimmerman−Traxler-type TS. Chiral-phosphate-dependent stereoselectivity arising from this TS is influenced by a hydrogen bond between the phosphoryl oxygen and the aldehyde formyl proton present in TADDOL-derived catalysts. This hydrogen bond is absent in the corresponding BINOL-derived systems because of a steric clash between the chiral phosphine and chiral phosphate ligands. Additional factors influencing the stereochemical control have been determined. Match/mismatch effects between the chiral phosphate ligand **1b** and the chiral phosphine ligands (*R*)- and (*S*)-SEGPHOS are qualitatively rationalized.

2. COMPUTATIONAL DETAILS

Quantum-mechanical calculations were performed using Gaussian 09 (revision D.01).[19] All of the geometries were optimized using the B3LYP density functional[20,21] with the SDD basis set for ruthenium and 6-31G(d) for all other atoms. Single-point energies were calculated using M06[22] within the IEFPCM model (acetone)[23] with a mixed basis set of SDD for ruthenium and 6-311G(d,p) for all other atoms. The resulting energies were used to correct the gas-phase energies obtained from the B3LYP calculations.[24−26] Previous computational studies of ruthenium catalysts with these methods provided results in accord with experiment.[27−29] Computed structures are illustrated with CYLView.[30]

The arrangement of ligands around ruthenium and the conformation of the phosphate ligand in our calculations were derived from the X-ray crystal structure of a TADDOL-derived catalyst system reported by Krische and co-workers.[11] TSs with other ligand arrangements were located using a model catalyst system (see the Supporting Information). The trans arrangement of the phosphate and CO ligands was found to be strongly favored over cis arrangements (by at least 13.5 kcal mol^{-1}). This is in agreement with structures reported for similar allylruthenium complexes, which show that CO and anionic ligands prefer to be trans.[31,32]

The chiral phosphates were truncated as outlined in Scheme 3 to simplify our calculations (**1b** and **2b**). Both of these truncated phosphates were tested experimentally under unoptimized conditions, and the truncation was reported to have a minimal effect on the reaction outcome (**1a** = 94% ee, 4.1:1 dr, **1b** = 90% ee, 3.0:1 dr;[11] **2a** = 72% ee, 4:1 dr, **2b** = 72% ee, 5:1 dr[10]). The aldehydes were also truncated to ethanal.[33,34]

3. RESULTS AND DISCUSSION

TADDOL-Derived Catalyst System. The orientation of the SEGPHOS phenyl groups are controlled by the ligand's C_2-symmetric nature (Figure 1a). The TADDOL framework adopts a "slanted" orientation with respect to the P−Ru−P plane, which makes interactions with the left-hand-side phenyl groups of SEGPHOS the most important (Figure 1b). The left, upward-pointing phenyl group of SEGPHOS occupies an empty quadrant of the TADDOL-derived scaffold, helping to restrict phosphate rotation (Figure 1c). The slanted nature of the phosphate also creates a network of CH−π interactions between the TADDOL-derived phosphate and the left-hand-side phenyl groups of SEGPHOS that increases the conformational rigidity of the catalyst structure (Figure 1d). Therefore, the chirality of the two ligands complement each other, which leads to a well-defined chiral pocket in the empty quadrant in which carbonyl crotylation can occur. (*R*)-SEGPHOS leads to lower enantioselectivity under unoptimized conditions ((*S*)-SEGPHOS = 89% ee, (*R*)-SEGPHOS = 31% ee). Qualitatively, this is expected to be the result of reduced catalyst conformational rigidity due to a mismatch between the SEGPHOS phenyl groups, which are now the mirror image of those shown in Figure 1a, and the slanted nature of the chiral phosphate, which disrupts the CH−π interactions and the intersection of the upward-pointing phenyl group of SEGPHOS with the TADDOL-derived scaffold. In the presence of an achiral phosphine (1,1′-bis(diphenylphosphino)-ferrocene (dppf)), modest enantioselectivity is observed under unoptimized conditions ((*S*)-SEGPHOS = 89% ee, dppf = 78% ee). In the absence of a rigid chiral ligand, the resulting increase in

DOI: 10.1021/jacs.5b04844
J. Am. Chem. Soc. 2015, 137, 8838−8850

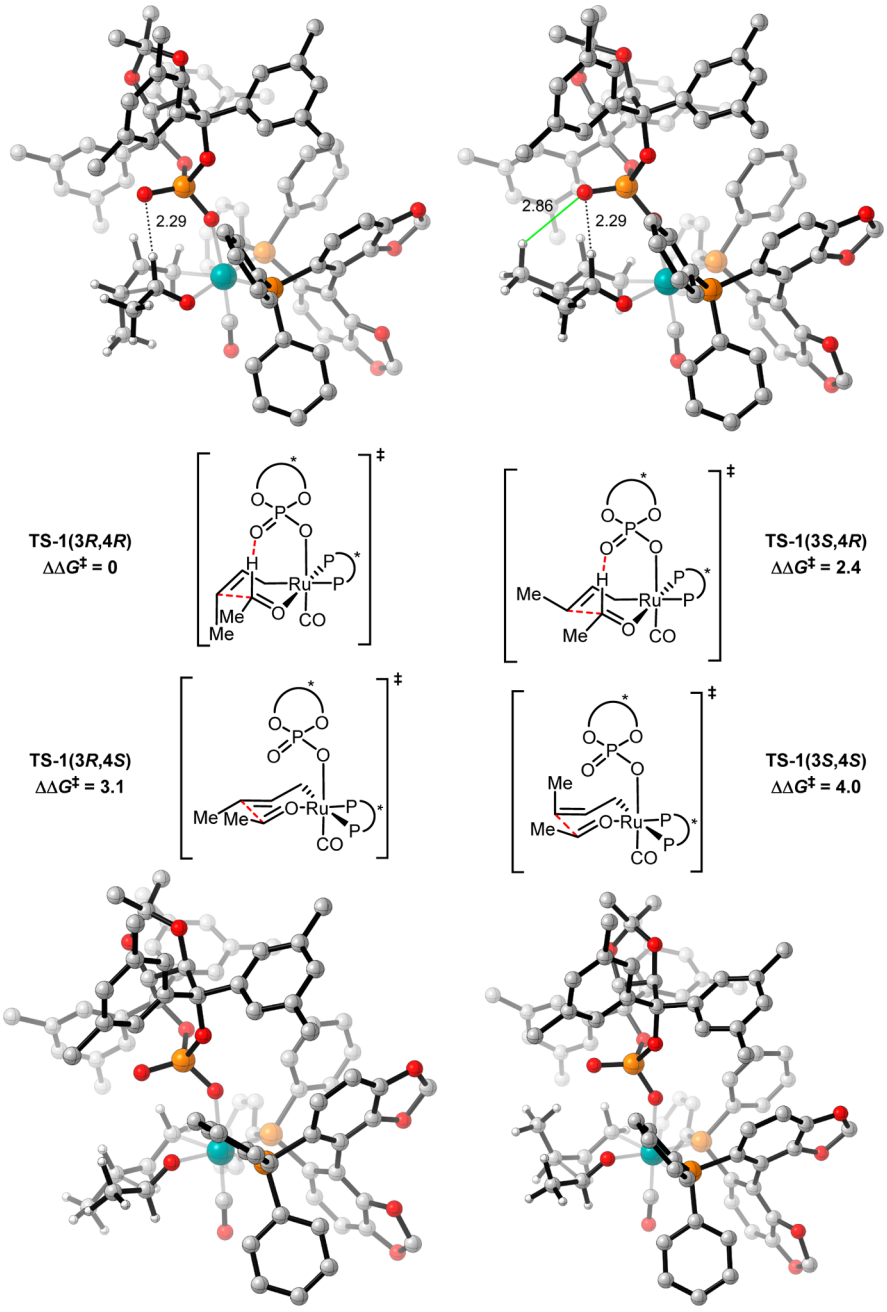

Figure 3. C−C bond-forming TSs for reaction 1. Free energies of activation relative to **TS-1(3*R*,4*R*)** are shown. M06/SDD-6-311G(d,p)−IEFPCM(acetone)//B3LYP/SDD-6-31G(d). Noncritical hydrogen atoms have been omitted for clarity. All free energies are in kcal mol^{-1}. **TS-1(3*S*,4*R*)** is destabilized relative to **TS-1(3*R*,4*R*)** by a phosphate−substrate steric interaction (green line in **TS-1(3*S*,4*R*)**) and gauche interactions.

Table 1. Comparison of C−C Bond-Forming TSs for Reaction 1 [(3*R*,4*R*) = Major Product; See Scheme 4 for Aldehyde Coordination Sites]

	TS	σ-crotylruthenium isomer	aldehyde R group	aldehyde coordination site	ΔΔG‡ (kcal mol^{-1})	CH···O	experimental product ratio
TS-1(3*R*,4*R*)	chair	*Z*	pseudoequatorial	1	0	yes	79
TS-1(3*S*,4*R*)	chair	*E*	pseudoequatorial	1	2.4	yes	12
TS-1(3*R*,4*S*)	chair	*E*	pseudoequatorial	1	3.1	no	7
TS-1(3*S*,4*S*)	chair	*Z*	pseudoequatorial	1	4.0	no	2

phosphine conformational flexibility is expected to lead to fluxional matching and mismatching between the phosphine and the TADDOL-derived framework and hence lower enantioselectivity.

The π-allyl species are expected to be the resting state of the catalytic cycle or close in energy to it.[12] To gain an insight into their structures, all eight possible π-allyl species were located. These arise from the following variables: π-crotylruthenium isomer (*syn* or *anti*) and α-methyl group orientation (toward or away from phosphate and left or right). For reaction 1 in Scheme 3, DFT calculations show that the thermodynamically preferred

DOI: 10.1021/jacs.5b04844
J. Am. Chem. Soc. 2015, 137, 8838−8850

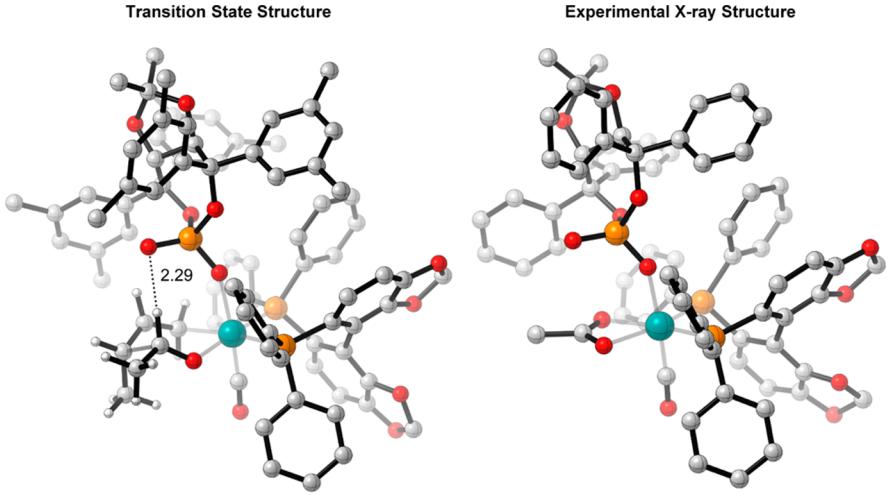

Figure 4. Comparison of **TS-1(3*R*,4*R*)** and the X-ray crystal structure of a related catalyst system. M06/SDD-6-311G(d,p)−IEFPCM(acetone)//B3LYP/SDD-6-31G(d). Noncritical hydrogen atoms have been omitted for clarity.

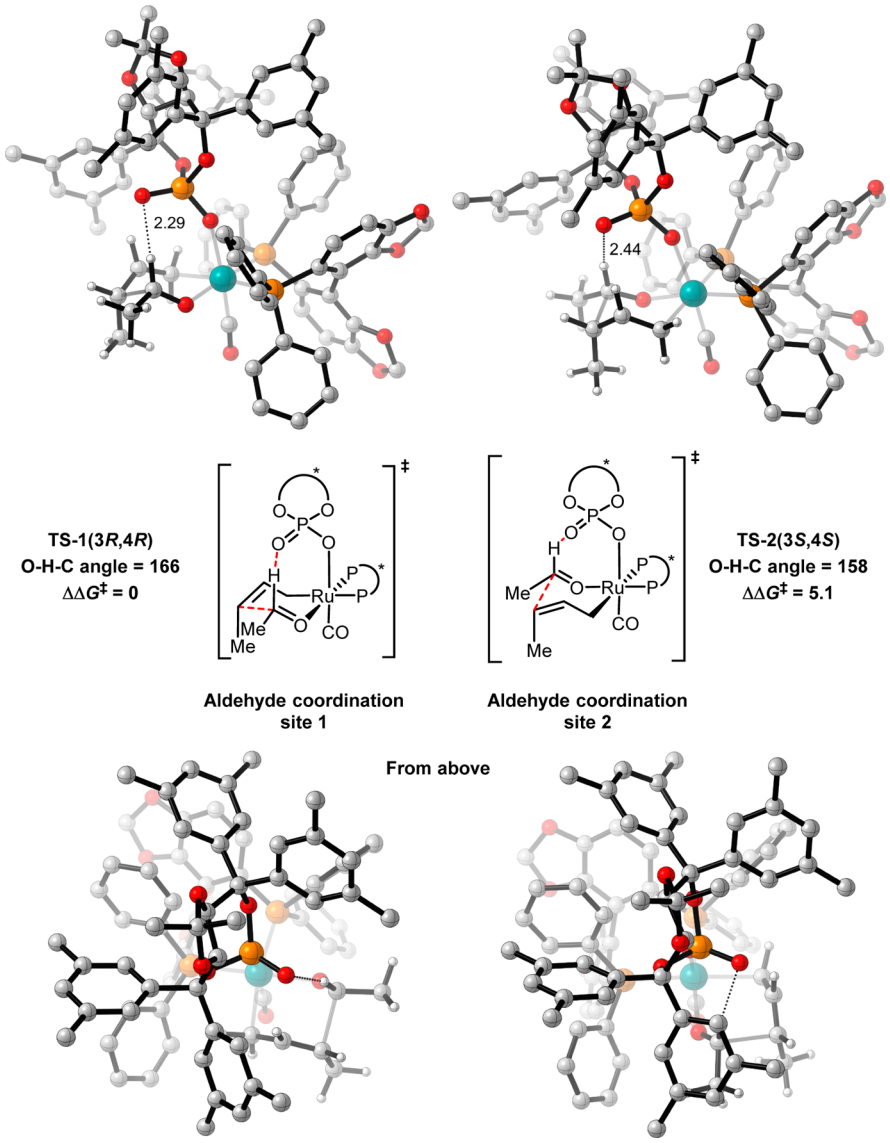

Figure 5. Comparison of aldehyde coordination sites in C−C bond-forming TSs for reaction 1. The O−H−C angle is the angle defined by the P═O oxygen and the aldehyde C−H. Free energies of activation relative to **TS-1(3*R*,4*R*)** are shown. M06/SDD-6-311G(d,p)−IEFPCM(acetone)//B3LYP/SDD-6-31G(d). Noncritical hydrogen atoms have been omitted for clarity. All free energies are in kcal mol^{-1}.

DOI: 10.1021/jacs.5b04844
J. Am. Chem. Soc. 2015, 137, 8838−8850

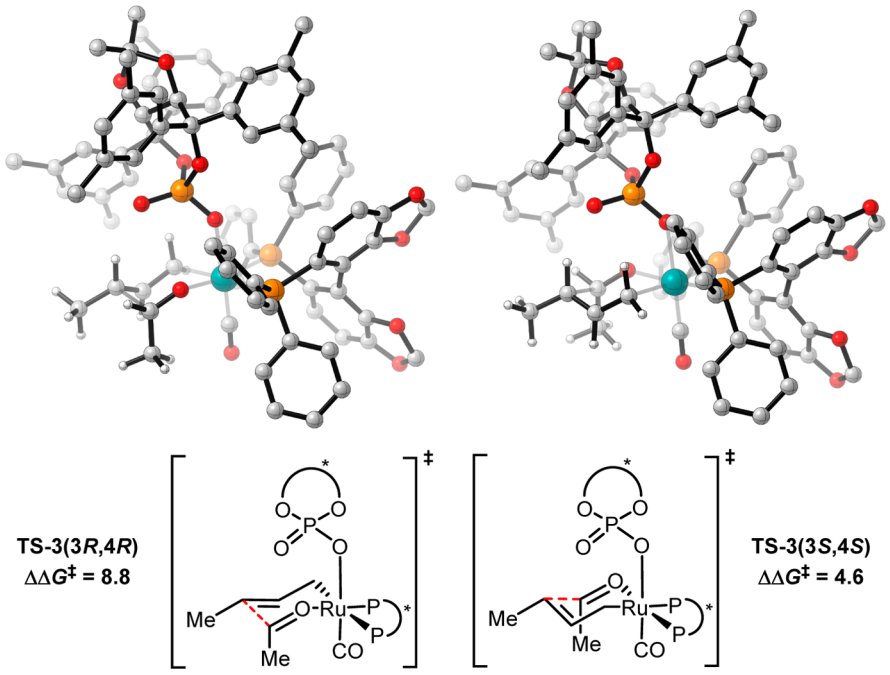

Figure 6. TS arrangements with the aldehyde substituent pseudoaxial and down and the crotyl methyl group pseudoequatorial for reaction 1. Free energies of activation relative to **TS-1(3*R*,4*R*)** are shown. M06/SDD-6-311G(d,p)−IEFPCM(acetone)//B3LYP/SDD-6-31G(d). Noncritical hydrogen atoms have been omitted for clarity. All free energies are in kcal mol^{-1}.

π-crotylruthenium isomer is the *syn*-π-allyl species by 6.4 kcal mol^{-1} (Figure 2). However, as described above, these π-allyl species are in rapid equilibrium, and their relative thermodynamic stabilities do not determine the diastereocontrol (Curtin−Hammett conditions).[35] Therefore, the kinetics of C−C bond formation were investigated.

All 16 possible chairlike C−C bond-forming TSs were located for reaction 1. These arise from the following variables: σ-crotylruthenium isomer (*E* or *Z*), aldehyde substituent orientation (toward or away from the phosphate and pseudoaxial or pseudoequatorial), and aldehyde coordination site (site 1 or 2; Scheme 4). All four (*Z*)-σ-crotylruthenium boatlike C−C bond-forming TSs with the aldehyde substituent pseudoequatorial were calculated to be strongly disfavored relative to the lowest-energy chairlike TS (by over 5 kcal mol^{-1}). Therefore, boatlike TSs were not investigated further. TSs with alternative P═O orientations leading to the major product were also explored but were calculated to be strongly disfavored relative to the TS in which the P═O is oriented over the substrate (by over 4 kcal mol^{-1}). Twenty-four unique TSs were found in total, with a free energy spread of 14.6 kcal mol^{-1}. The four TSs that led to each of the experimentally observed products are shown in Figure 3 and Table 1. These are all lower in energy than different TSs leading to the same product by at least 0.9 kcal mol^{-1}.

The lowest-energy TS, **TS-1(3*R*,4*R*)**, leads to the major product observed experimentally. From the lowest-energy *syn*-π-allyl species, the barrier to this TS is 24.3 kcal mol^{-1}. In both **TS-1(3*R*,4*R*)** and **TS-1(3*S*,4*R*)**, there is a hydrogen-bonding interaction from the catalyst phosphoryl oxygen to the aldehyde formyl proton. The formyl hydrogen bond has previously been identified to play a crucial role in phosphoric acid-catalyzed asymmetric aldehyde allylboration and allenylboration, and in these reactions this interaction is calculated to be worth approximately 3 kcal mol^{-1}.[36,37] The H···O distances in **TS-1(3*R*,4*R*)** and **TS-1(3*S*,4*R*)** (2.3 Å) are similar to those observed in asymmetric aldehyde allylboration and allenylboration (∼2.2 Å). The lower energy of the (*Z*)-σ-crotylruthenium TS (**TS-1(3*R*,4*R*)**) relative to the (*E*)-σ-crotylruthenium TS (**TS-1(3*S*,4*R*)**) is unexpected, as the former TS places the crotyl methyl group pseudoaxially. However, doing so minimizes gauche interactions between this group and the aldehyde substituent, as has been found in certain aldol reactions.[38] Furthermore, the crotyl methyl group's proximity to the chiral phosphate also contributes to destabilization of **TS-1(3*S*,4*R*)** (Figure 3). Therefore, the unexpected diastereoselectivity is both a catalyst and a substrate effect.

TS-1(3*R*,4*S*) and **TS-1(3*S*,4*S*)** are destabilized relative to **TS-1(3*R*,4*R*)** and **TS-1(3*S*,4*R*)** because of the absence of the formyl hydrogen bond. **TS-1(3*S*,4*S*)** is further destabilized as a result of the proximity of the pseudoaxial methyl group to the chiral phosphate. This leads to the high levels of enantiocontrol observed experimentally. The computed enantioselectivity arising from **TS-1(3*R*,4*R*)** and **TS-1(3*S*,4*S*)** is predicted to be 99% at 368 K, somewhat higher than that seen experimentally (95%).

The calculated TSs closely resemble the experimental X-ray crystal structure reported for a related catalyst system (Figure 4).[11] To further confirm DFT's ability to model this type of catalyst system, the catalyst structure was optimized (M06/SDD-6-311G(d,p)−IEFPCM(acetone)//B3LYP/SDD-6-31G(d)) starting from the experimental X-ray crystal structure. Superposition of ruthenium and its six surrounding atoms from the calculated and experimental structures led to a root-mean-square deviation (RMSD) of 0.08 Å. This shows that computation and experiment are in excellent agreement.

Coordination of the aldehyde to site 2 leads to formyl hydrogen bond lengthening and directional distortion (**TS-2(3*S*,4*S*)**; Figure 5). Also, the steric clash between the aldehyde and the aromatic group of the TADDOL framework is much greater in coordination mode 2 than the clash between the σ-crotylruthenium species and the same aromatic group in coordination mode 1 because of the orientation of the chairlike TS ("From above" in Figure 5). Both of these factors destabilize **TS-2(3*S*,4*S*)** relative to **TS-1(3*R*,4*R*)**. Under unoptimized

DOI: 10.1021/jacs.5b04844
J. Am. Chem. Soc. 2015, 137, 8838−8850

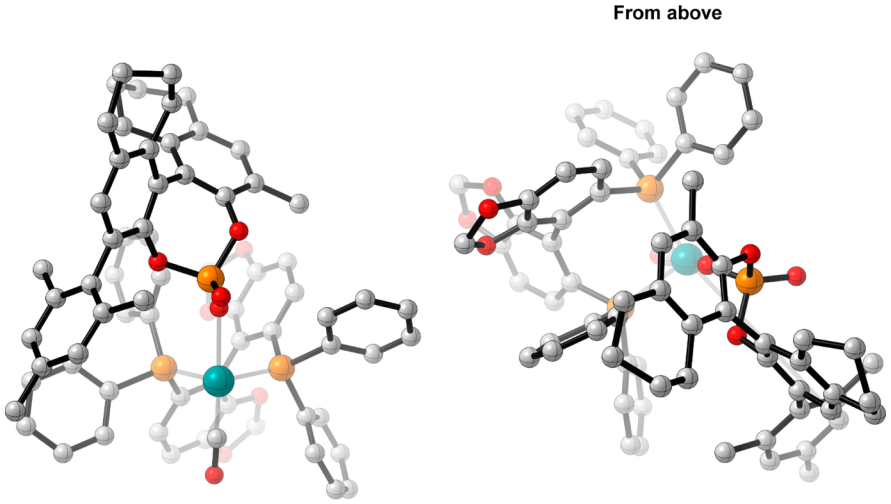

Figure 7. Different views of the BINOL-derived catalyst system. All of the structures are derived from optimized *syn*-π-allyl species; noncritical atoms have been omitted for clarity. M06/SDD-6-311G(d,p)−IEFPCM(acetone)//B3LYP/SDD-6-31G(d).

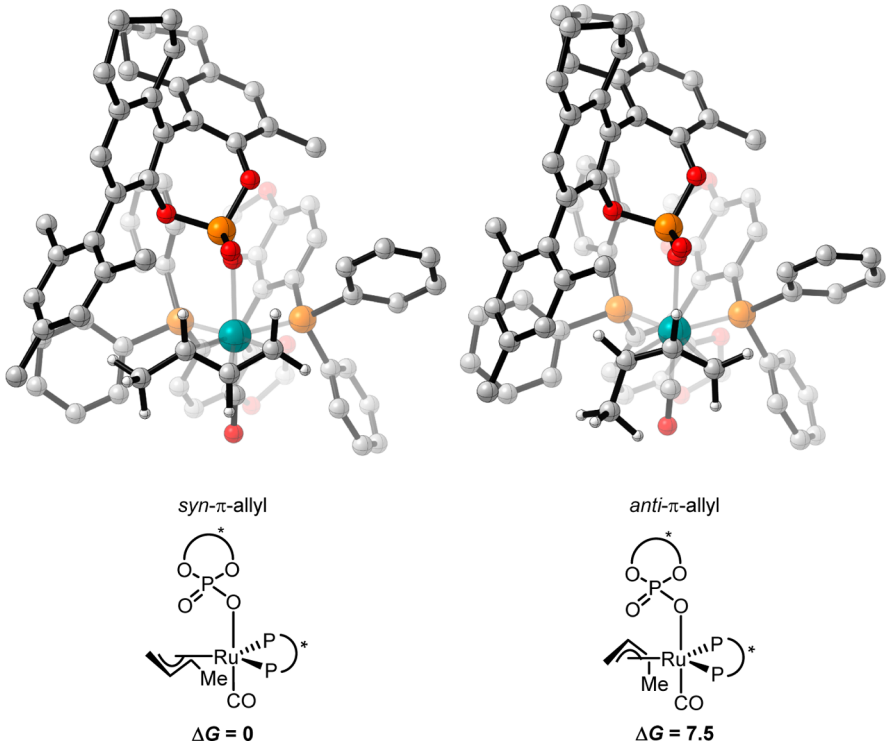

Figure 8. Lowest-energy *syn*- and *anti*-π-crotylruthenium isomers in reaction 2. M06/SDD-6-311G(d,p)−IEFPCM(acetone)//B3LYP/SDD-6-31G(d). Noncritical hydrogen atoms have been omitted for clarity. All free energies are in kcal mol^{-1}.

conditions, switching the chiral phosphate's substituent from *m*-xylyl to methyl leads to a decrease of 77% in the enantioselectivity. Qualitatively, upon removal of the sterically demanding aromatic substituents, coordination of the aldehyde to site 2 would be expected to become comparable to that at site 1, which would lead to a large drop in ee.

The TSs leading to the minor diastereomers via the (*Z*)-σ-crotylruthenium isomer are chairlike with the aldehyde substituent pseudoaxial, or boatlike, and both are higher in energy than **TS-1(3*S*,4*S*)**. If only the (*Z*)-σ-crotylruthenium isomer were present in solution, higher levels of diastereoselectivity than enantioselectivity would be observed. This is consistent with the very high levels of diastereocontrol observed in aldehyde crotylboration when a single crotylboronate isomer is employed.[39] Our calculations support experimental evidence showing that rapid isomerization between π-allyl species occurs to form both σ-crotylruthenium isomers.[16−18]

TS arrangements with the aldehyde substituent pseudoaxial and down and the crotyl methyl group pseudoequatorial are disfavored relative to **TS-1(3*R*,4*R*)** because of loss of the formyl hydrogen bond and the steric clash of the aldehyde substituent with the CO ligand and phosphine in **TS-3(3*R*,4*R*)** and with CO and the TADDOL-derived scaffold in **TS-3(3*S*,4*S*)** (Figure 6).

BINOL-Derived Catalyst System. The BINOL-derived scaffold is much longer and more rigid than its TADDOL counterpart (Figure 7). A projection from above shows that the

DOI: 10.1021/jacs.5b04844
J. Am. Chem. Soc. 2015, 137, 8838−8850

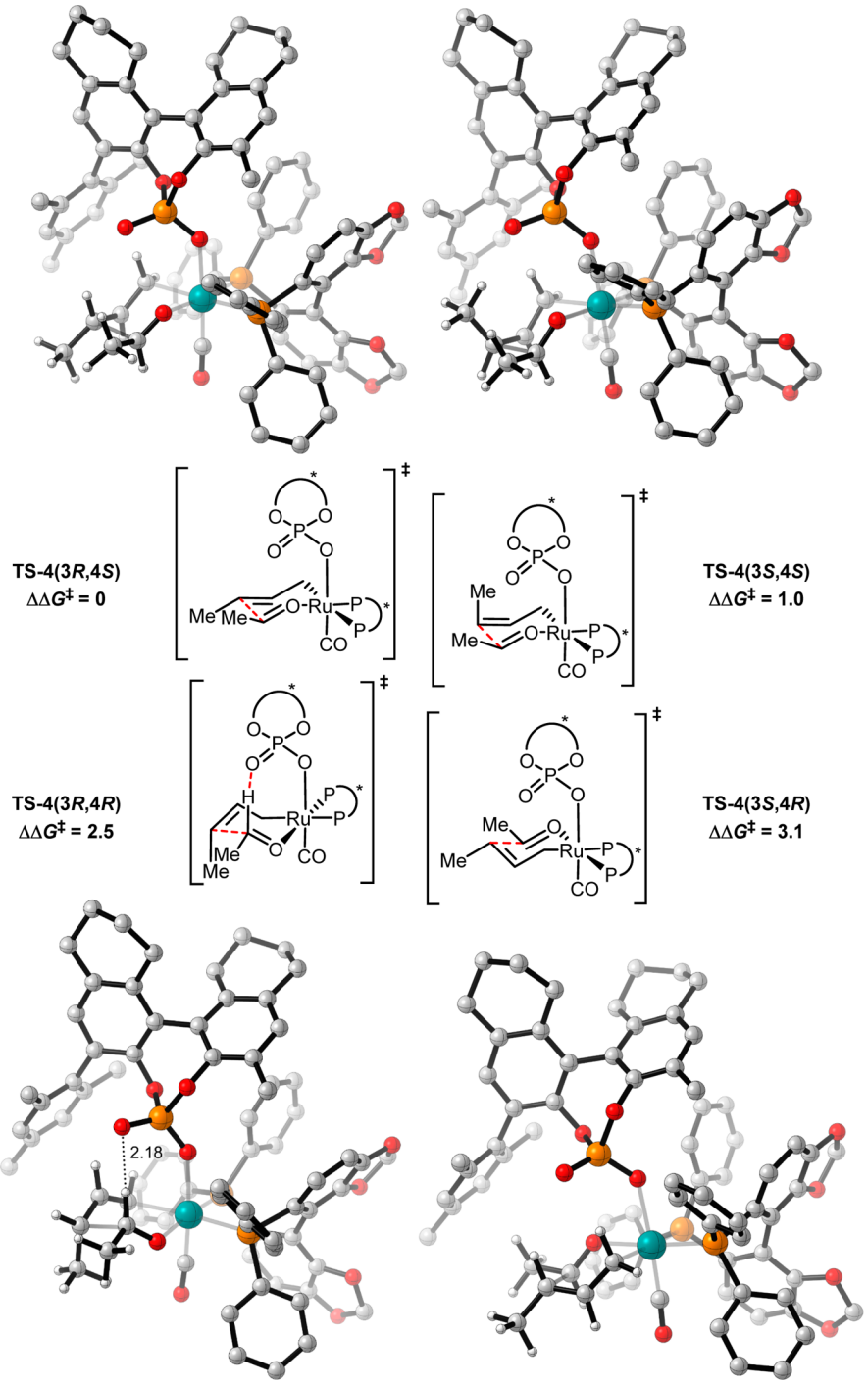

Figure 9. C−C bond-forming TSs for reaction 2. Free energies of activation relative to **TS-4(3*R*,4*S*)** are shown. M06/SDD-6-311G(d,p)−IEFPCM(acetone)//B3LYP/SDD-6-31G(d). Noncritical hydrogen atoms have been omitted for clarity. All free energies are in kcal mol^{-1}.

BINOL-derived phosphate does not intersect the SEGPHOS ligand like the TADDOL-derived phosphate does ("From above" in Figure 7). Instead, SEGPHOS acts as a steric barrier, restricting rotation of the BINOL-derived ligand. This implies that the chiral nature of SEGPHOS is less important relative to the TADDOL-derived system, which may be why BINOL-derived ligands have been found to give excellent levels of enantiocontrol in the absence of a chiral phosphine (Scheme 2).[10]

As before, the π-allyl species are expected to be the resting state of the catalytic cycle or close in energy to it.[12] The eight possible π-allyl species once again arise from the following variables: π-crotylruthenium isomer (*syn* or *anti*) and α-methyl group orientation (toward or away from the phosphate and left or right). For reaction 2 in Scheme 3, DFT calculations show that the thermodynamically preferred π-crotylruthenium isomer is the *syn*-π-allyl species by 7.5 kcal mol^{-1} (Figure 8). However, as described above, these π-allyl species are in rapid equilibrium, and their relative thermodynamic stabilities do not determine the diastereocontrol (Curtin−Hammett conditions).[35] Therefore, the kinetics of C−C bond formation were investigated.

The 16 possible chairlike C−C bond-forming TSs for reaction 2 once again arise from the following variables: σ-crotylruthenium

DOI: 10.1021/jacs.5b04844
J. Am. Chem. Soc. 2015, 137, 8838−8850

Table 2. Comparison of C−C Bond-Forming TSs for Reaction 2 [(3*R*,4*S*) = Major Product; See Scheme 4 for Aldehyde Coordination Sites]

	TS	σ-crotylruthenium isomer	aldehyde R group	Aldehyde coordination site	$\Delta\Delta G^{\ddagger}$ (kcal mol^{-1})	CH···O	experimental product ratio
TS-4(3*R*,4*S*)	chair	*E*	pseudoequatorial	1	0	no	65
TS-4(3*S*,4*S*)	chair	*Z*	pseudoequatorial	1	1.0	no	15
TS-4(3*R*,4*R*)	chair	*Z*	pseudoequatorial	1	2.5	yes	17
TS-4(3*S*,4*R*)	chair	*E*	pseudoequatorial	2	3.1	no	3

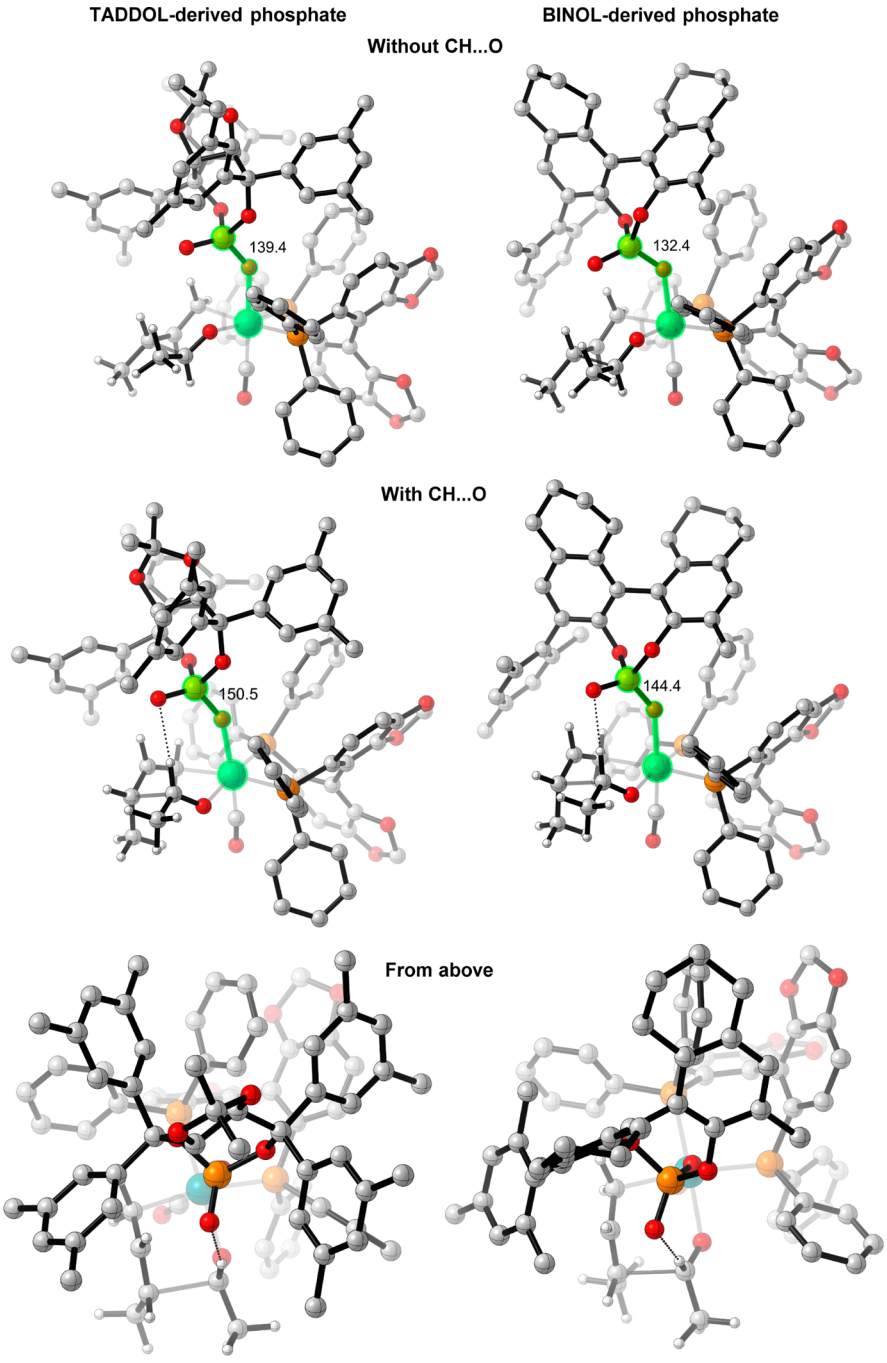

Figure 10. Comparison of TSs with and without the formyl hydrogen bond. M06/SDD-6-311G(d,p)−IEFPCM(acetone)//B3LYP/SDD-6-31G(d). The measured angle is highlighted in green. Noncritical hydrogen atoms have been omitted for clarity.

isomer (*E* or *Z*), aldehyde substituent orientation (toward or away from the phosphate and pseudoaxial or pseudoequatorial), and aldehyde coordination site (site 1 or 2; Scheme 4). All eight chairlike C−C bond-forming TSs (aldehyde substituent fixed as pseudoequatorial) with an alternative orientation of the C_1-symmetric BINOL-derived ligand were also considered (*vide infra*, Figure 11). Twenty-eight unique TSs were located in total. The four TSs that led to

DOI: 10.1021/jacs.5b04844
J. Am. Chem. Soc. 2015, 137, 8838−8850

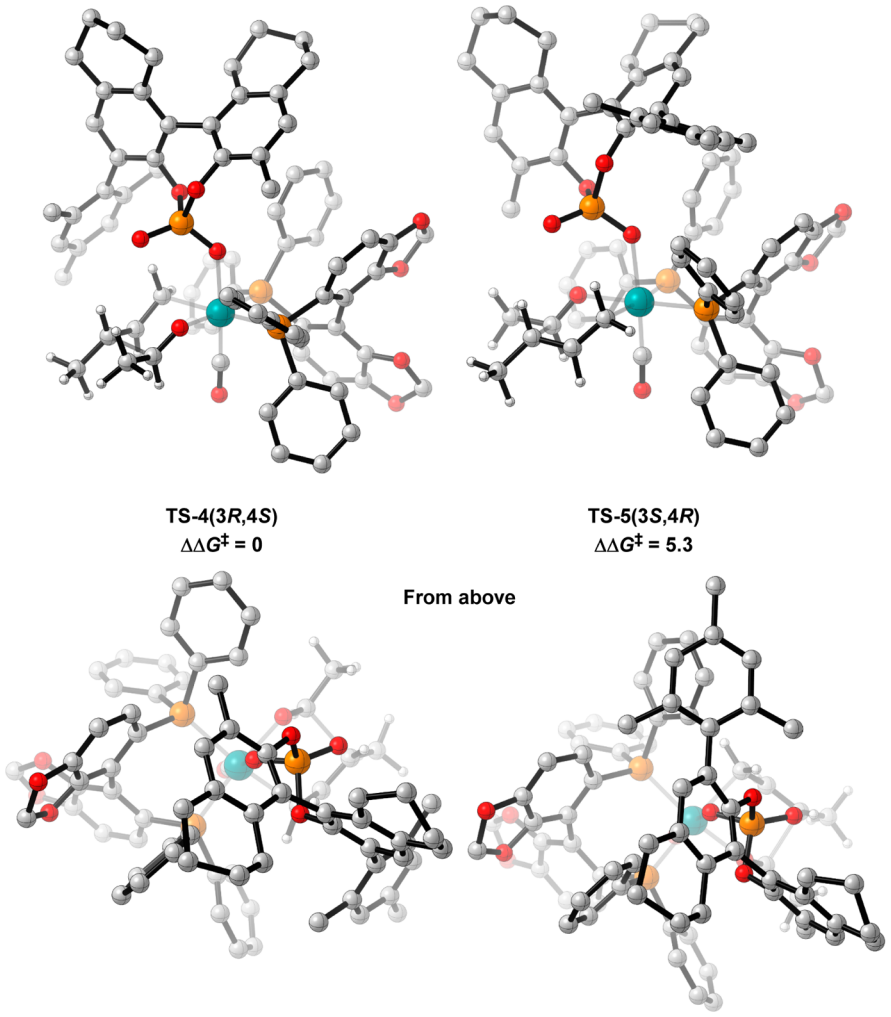

Figure 11. TSs with different conformations of the C_1-symmetric BINOL-derived ligand. Free energies of activation relative to **TS-4(3*R*,4*S*)** are shown. M06/SDD-6-311G(d,p)−IEFPCM(acetone)//B3LYP/SDD-6-31G(d). Noncritical hydrogen atoms have been omitted for clarity. All free energies are in kcal mol^{-1}.

each of the experimentally observed products are shown in Figure 9 and Table 2.

The lowest energy TS is **TS-4(3*R*,4*S*)**, which leads to the major product observed experimentally. From the lowest-energy π-allyl species, the barrier to this TS is 23.1 kcal mol^{-1}. Preferentially, in both of the most-favored TSs (**TS-4(3*R*,4*S*)** and **TS-4(3*S*,4*S*)**), the formyl hydrogen bond that was observed in reaction 1 is now absent in reaction 2. **TS-4(3*R*,4*R*)** is the lowest-energy TS that contains the formyl hydrogen bond, but it is destabilized by 2.5 kcal mol^{-1} relative to **TS-4(3*R*,4*S*)**. The lack of this interaction upon changing the phosphate ligand can be rationalized by considering projections of the TSs from above (Figure 10). In order to establish this hydrogen-bonding interaction, the chiral phosphate must pivot back toward the phosphine and increase the Ru−O−P angle. When the hydrogen bond is absent, this angle is 139° and 132° in **TS-1(3*R*,4*S*)** and **TS-4(3*R*,4*S*)**, respectively. When the hydrogen bond is present, this angle increases to 150° and 144° in **TS-1(3*R*,4*R*)** and **TS-4(3*R*,4*R*)**, respectively. In the projections of the TSs from above, looking down on the hydrogen bond, the TADDOL framework can be seen to fit between the steric demands of SEGPHOS and can easily accommodate the increase in the Ru−O−P angle ("From above" in Figure 10). However, the BINOL framework is oriented directly toward a phenyl group of SEGPHOS, making this increase in the Ru−O−P angle more unfavorable. This catalyst distortion overrides the benefit from the formyl hydrogen bond. Also, H_8-BINOL-derived phosphoric acids are more acidic than their TADDOL counterparts by approximately 2 pK_a units in dimethyl sulfoxide.[40] The enhanced Lewis basicity of the TADDOL-derived phosphate might contribute to a more favorable formyl hydrogen bond.

The lack of formyl hydrogen bond in reaction 2 and the steric preference for a different TS explain why nucleophilic attack occurs on the opposite face of the prochiral aldehyde relative to reaction 1. The *syn*-diastereoselectivity is lost, as the pseudoaxial methyl group now points directly toward the phosphate moiety (**TS-4(3*S*,4*S*)**). The lowest-energy TS is **TS-4(3*R*,4*S*)** despite the unfavorable gauche interactions between the methyl groups. Higher levels of diastereocontrol are observed in the reaction of aromatic aldehydes with a related BINOL-derived catalyst system (Scheme 2).[10] This is the case because these substrates minimize gauche interactions in the C−C bond-forming TS. Furthermore, unlike **TS-1(3*S*,4*R*)**, which is partly destabilized by the proximity of the crotyl methyl group to the chiral phosphate, this methyl group in **TS-4(3*R*,4*S*)** is directed down, away from the phosphate moiety.

TS-4(3*S*,4*R*), leading to the minor enantiomer, involves coordination of the aldehyde to site 2. This arrangement avoids the

DOI: 10.1021/jacs.5b04844
J. Am. Chem. Soc. 2015, 137, 8838−8850

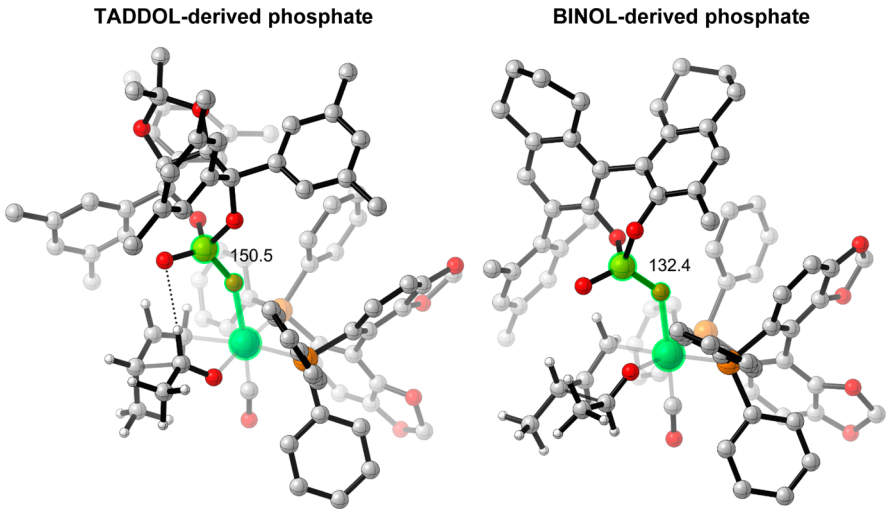

Figure 12. Lowest-energy C−C bond-forming TSs for reactions 1 and 2. M06/SDD-6-311G(d,p)−IEFPCM(acetone)//B3LYP/SDD-6-31G(d). Noncritical hydrogen atoms have been omitted for clarity.

formyl hydrogen bond but is destabilized relative to **TS-4(3*R*,4*S*)** as a result of unfavorable steric interactions with the chiral phosphate. This leads to the high levels of enantiocontrol observed experimentally. The computed enantioselectivity arising from **TS-4(3*R*,4*S*)** and **TS-4(3*S*,4*R*)** was found to be 97% at 378 K, somewhat higher than that seen experimentally (91%). The lower enantioselectivity observed experimentally for this system relative to the TADDOL-derived catalyst is reproduced by our calculations. Under unoptimized conditions with an achiral phosphine ligand, switching the chiral phosphate's substituent from mesityl to phenyl leads to a decrease of 36% in the enantioselectivity (with the naphthyl alkyl group of the catalyst replaced by hydrogen in both cases). Qualitatively, upon reduction of the steric demands of the aromatic substituent, coordination of the aldehyde to site 2 would be expected to become comparable to that at site 1, which would lead to a drop in ee.

Eight chairlike C−C bond-forming TSs (with the aldehyde substituent fixed as pseudoequatorial) with an alternative orientation of the C_1-symmetric BINOL-derived ligand were located. The lowest-energy TS with this alternative arrangement, **TS-5(3*S*,4*R*)**, was found to be disfavored by 5.3 kcal mol^{-1} relative to **TS-4(3*R*,4*S*)** because of a steric clash between the 2,4,6-trimethylphenyl substituent of the naphthyl ring and a SEGPHOS phenyl group (Figure 11).

4. CONCLUSIONS

DFT calculations show that C−C bond formation in the ruthenium-catalyzed asymmetric hydrohydroxyalkylation of butadiene occurs via a closed-chair Zimmerman−Traxler-type TS. Match/mismatch effects between the chiral phosphate ligand **1b** and the chiral phosphine ligands (*R*)- and (*S*)-SEGPHOS are qualitatively rationalized. The chiral-phosphate-dependent stereoselectivity is the result of a hydrogen bond between the phosphoryl oxygen and the aldehyde formyl proton that is present in TADDOL-derived catalysts but absent in the corresponding BINOL-derived systems because of a steric clash between the chiral phosphine and chiral phosphate ligands.

With this hydrogen bond in place, the *syn*-diastereoselectivity with TADDOL-derived catalysts arises from preferential reaction of the (*Z*)-σ-crotylruthenium isomer; this places the crotyl methyl group pseudoaxially to minimize gauche interactions between this group and the aldehyde (Figure 12). Because the formyl hydrogen bond cannot be achieved without catalyst distortion in BINOL-derived systems, nucleophilic attack occurs on the opposite face of the prochiral aldehyde. Also, the *syn*-diastereoselectivity is lost, as the pseudoaxial methyl group now points directly toward the phosphate moiety. Therefore, the lowest-energy TS leads to *anti*-diastereoselectivity despite the unfavorable gauche interactions between the methyl groups (Figure 12). The lower enantioselectivity observed experimentally for this system relative to the TADDOL-derived catalyst (91 vs 95% ee, respectively) is reproduced by our calculations (97 vs 99% ee, respectively).

■ ASSOCIATED CONTENT

Supporting Information

Complete list of authors in the Gaussian 09 reference (ref 19); Cartesian coordinates, energies, free energies, and numbers of imaginary frequencies for all stationary points and values of the imaginary frequencies for all transition structures. The Supporting Information is available free of charge on the ACS Publications website at DOI: 10.1021/jacs.5b04844.

■ AUTHOR INFORMATION

Corresponding Author

*houk@chem.ucla.edu

Notes

The authors declare no competing financial interest.

■ ACKNOWLEDGMENTS

We are grateful to The English-Speaking Union (Lindemann Trust Fellowship to M.N.G.), the NIH-NIGMS (RO1-GM069445 to M.J.K.), and the NSF (CHE-1361104 to K.N.H.) for financial support. Computational resources were provided by the UCLA Institute for Digital Research and Education (IDRE) and the Extreme Science and Engineering Discovery Environment (XSEDE), which is supported by the NSF (OCI-1053575).

■ REFERENCES

(1) Yamamoto, Y.; Asao, N. *Chem. Rev.* **1993**, *93*, 2207−2293.
(2) Marek, I.; Sklute, G. *Chem. Commun.* **2007**, 1683−1691.
(3) Yus, M.; González-Gómez, J. C.; Foubelo, F. *Chem. Rev.* **2011**, *111*, 7774−7854.

DOI: 10.1021/jacs.5b04844
J. Am. Chem. Soc. 2015, 137, 8838−8850

(4) Yus, M.; González-Gómez, J. C.; Foubelo, F. *Chem. Rev.* **2013**, *113*, 5595−5698.
(5) Dechert-Schmitt, A.-M. R.; Schmitt, D. C.; Gao, X.; Itoh, T.; Krische, M. J. *Nat. Prod. Rep.* **2014**, *31*, 504−513.
(6) Kennedy, J. W. J.; Hall, D. G. *Angew. Chem., Int. Ed.* **2003**, *42*, 4732−4739.
(7) Denmark, S. E.; Fu, J. *Chem. Rev.* **2003**, *103*, 2763−2794.
(8) Brown, H. C.; Bhat, K. S. *J. Am. Chem. Soc.* **1986**, *108*, 293−294.
(9) Brown, H. C.; Bhat, K. S. *J. Am. Chem. Soc.* **1986**, *108*, 5919−5923.
(10) Zbieg, J. R.; Yamaguchi, E.; McInturff, E. L.; Krische, M. J. *Science* **2012**, *336*, 324−327.
(11) McInturff, E. L.; Yamaguchi, E.; Krische, M. J. *J. Am. Chem. Soc.* **2012**, *134*, 20628−20631.
(12) Li, H.; Wang, Z.-X. *Organometallics* **2012**, *31*, 2066−2077.
(13) Xue, P.; Bi, S.; Sung, H. H. Y.; Williams, I. D.; Lin, Z.; Jia, G. *Organometallics* **2004**, *23*, 4735−4743.
(14) Silva, L. C.; Gomes, P. T.; Veiros, L. F.; Pascu, S. I.; Duarte, M. T.; Namorado, S.; Ascenso, J. R.; Dias, A. R. *Organometallics* **2006**, *25*, 4391−4403.
(15) Zimmerman, H. E.; Traxler, M. D. *J. Am. Chem. Soc.* **1957**, *79*, 1920−1923.
(16) Chen, T.-Y.; Tsutsumi, R.; Montgomery, T. P.; Volchkov, I.; Krische, M. J. *J. Am. Chem. Soc.* **2015**, *137*, 1798−1801.
(17) Liang, T.; Nguyen, K. D.; Zhang, W.; Krische, M. J. *J. Am. Chem. Soc.* **2015**, *137*, 3161−3164.
(18) Zbieg, J. R.; McInturff, E. L.; Leung, J. C.; Krische, M. J. *J. Am. Chem. Soc.* **2011**, *133*, 1141−1144.
(19) Frisch, M. J.; et al. *Gaussian 09*, revision D.01; Gaussian, Inc.: Wallingford, CT, 2013.
(20) Becke, A. D. *Phys. Rev. A: At., Mol., Opt. Phys.* **1988**, *38*, 3098−3100.
(21) Lee, C.; Yang, W.; Parr, R. G. *Phys. Rev. B: Condens. Matter Mater. Phys.* **1988**, *37*, 785−789.
(22) Zhao, Y.; Truhlar, D. *Theor. Chem. Acc.* **2008**, *120*, 215−241.
(23) Tomasi, J.; Mennucci, B.; Cammi, R. *Chem. Rev.* **2005**, *105*, 2999−3093.
(24) Simón, L.; Goodman, J. M. *Org. Biomol. Chem.* **2011**, *9*, 689−700.
(25) Grayson, M. N.; Goodman, J. M. *J. Org. Chem.* **2015**, *80*, 2056−2061.
(26) Overvoorde, L. M.; Grayson, M. N.; Luo, Y.; Goodman, J. M. *J. Org. Chem.* **2015**, *80*, 2634−2640.
(27) Miyazaki, H.; Herbert, M. B.; Liu, P.; Dong, X.; Xu, X.; Keitz, B. K.; Ung, T.; Mkrtumyan, G.; Houk, K. N.; Grubbs, R. H. *J. Am. Chem. Soc.* **2013**, *135*, 5848−5858.
(28) Yang, Y.-F.; Chung, L. W.; Zhang, X.; Houk, K. N.; Wu, Y.-D. *J. Org. Chem.* **2014**, *79*, 8856−8864.
(29) Cannon, J. S.; Zou, L.; Liu, P.; Lan, Y.; O'Leary, D. J.; Houk, K. N.; Grubbs, R. H. *J. Am. Chem. Soc.* **2014**, *136*, 6733−6743.
(30) Legault, C. Y. *CYLView*, version 1.0b; Université de Sherbrooke: Sherbrooke, QC, Canada, 2009; http://www.cylview.org.
(31) Barnard, C. F. J.; Daniels, J. A.; Holland, P. R.; Mawby, R. J. *J. Chem. Soc., Dalton Trans.* **1980**, 2418.
(32) Chamberlain, B.; Duckett, S. B.; Lowe, J. P.; Mawby, R. J.; Stott, J. C. *Dalt. Trans.* **2003**, 2603.
(33) Williams, V. M.; Kong, J. R.; Ko, B. J.; Mantri, Y.; Brodbelt, J. S.; Baik, M.-H.; Krische, M. J. *J. Am. Chem. Soc.* **2009**, *131*, 16054−16062.
(34) Dugas, G. J.; Lam, Y.; Houk, K. N.; Krauss, I. J. *J. Org. Chem.* **2014**, *79*, 4277−4284.
(35) Seeman, J. I. *Chem. Rev.* **1983**, *83*, 83−134.
(36) Grayson, M. N.; Pellegrinet, S. C.; Goodman, J. M. *J. Am. Chem. Soc.* **2012**, *134*, 2716−2722.
(37) Grayson, M. N.; Goodman, J. M. *J. Am. Chem. Soc.* **2013**, *135*, 6142−6148.
(38) Lam, Y.; Houk, K. N.; Scheffler, U.; Mahrwald, R. *J. Am. Chem. Soc.* **2012**, *134*, 6286−6295.
(39) Jain, P.; Antilla, J. C. *J. Am. Chem. Soc.* **2010**, *132*, 11884−11886.
(40) Yang, C.; Xue, X.-S.; Jin, J.-L.; Li, X.; Cheng, J.-P. *J. Org. Chem.* **2013**, *78*, 7076−7085.

DOI: 10.1021/jacs.5b04844
J. Am. Chem. Soc. 2015, 137, 8838−8850